

Depth-dependent magnetic crossover in a room-temperature skyrmion-hosting multilayer

T. J. Hicken,^{1,2,3} M. N. Wilson,^{1,4} Z. Salman,³ S. L. Zhang,⁵ S. J. R. Holt,⁶
T. Prokscha,³ A. Suter,³ F. L. Pratt,⁷ G. van der Laan,⁸ T. Hesjedal,⁹ and T. Lancaster¹

¹*Department of Physics, Centre for Materials Physics,
Durham University, Durham, DH1 3LE, United Kingdom*

²*Department of Physics, Royal Holloway, University of London, Egham, TW20 0EX, United Kingdom*

³*Paul Scherrer Institute, Forschungsstrasse 111, 5232 Villigen PSI, Switzerland*

⁴*Department of Physics and Physical Oceanography,
Memorial University of Newfoundland, St. John's, NL A1B 3X7, Canada*

⁵*School of Physical Science and Technology, ShanghaiTech University,
Shanghai, 201210, China; ShanghaiTech Laboratory for Topological Physics,
ShanghaiTech University, Shanghai 200031, China*

⁶*Max Planck Institute for the Structure and Dynamics of Matter,
Luruper Chaussee 149, 22761 Hamburg, Germany*

⁷*ISIS Pulsed Neutron and Muon Facility, STFC Rutherford Appleton Laboratory,
Harwell Oxford, Didcot, OX11 0QX, United Kingdom*

⁸*Diamond Light Source, Harwell Science and Innovation Campus,
Didcot, Oxfordshire, OX11 0DE, United Kingdom*

⁹*Department of Physics, Clarendon Laboratory, University of Oxford, Oxford, OX1 3PU, United Kingdom*

(Dated: March 28, 2024)

Skyrmion-hosting multilayer stacks are promising avenues for applications, although little is known about the depth dependence of the magnetism. We address this by reporting the results of circular dichroic resonant elastic x-ray scattering (CD-REXS), micromagnetic simulations, and low-energy muon-spin rotation (LE- μ^+ SR) measurements on a stack comprising $[\text{Ta}/\text{CoFeB}/\text{MgO}]_{16}/\text{Ta}$ on a Si substrate. Energy-dependent CD-REXS shows a continuous, monotonic evolution of the domain-wall helicity angle with incident energy, consistent with a three-dimensional hybrid domain-wall-like structure that changes from Néel-like near the surface to Bloch-like deeper within the sample. LE- μ^+ SR reveals that the magnetic field distribution in the trilayers near the surface of the stack is distinct from that in trilayers deeper within the sample. Our micromagnetic simulations support a quantitative analysis of the μ^+ SR results. By increasing the applied magnetic field, we find a reduction in the volume occupied by domain walls at all depths, consistent with a crossover into a region dominated by skyrmions above approximately 180 mT.

I. INTRODUCTION

Several material classes have emerged that host magnetic skyrmion excitations [1, 2], but for applications it is necessary to stabilise skyrmions at room temperature. For this purpose, multilayer systems show promise [3]. These comprise a repeated stack of a magnetic layer and one or more heavy elements, e.g. Ta/CoFeB/MgO. Here, a Dzyaloshinskii-Moriya interaction (DMI) arises from inversion symmetry-breaking at interfaces between the layers, leading to skyrmions that can exist over a wide range of temperature, extending up to 500 K [4]. While skyrmions are often assumed to be a quasi-two-dimensional texture that identically repeats in the third dimension, recent work on Ta/CoFeB/MgO multilayers suggests a variation of the spin texture across multiple repeats of the multilayer [5], with micromagnetic simulations predicting that the helicity changes from Néel-type at the surface, to Bloch-type deeper in the stack.

There are many different techniques with which one can characterise three-dimensional spin textures such as skyrmions, which all have different strengths and weaknesses [6–16]. In the case of Ta/CoFeB/MgO multilayer stacks, circular dichroic resonant elastic x-ray scattering

(CD-REXS) measurements [17–19] have previously been employed to study the system [5, 20–22]. In this system, alternating non-magnetic spacers establish a pronounced dipole-dipole interaction among the CoFeB layers, leading to a unique hybrid three-dimensional (3D) domain wall configuration with a Bloch layer that is located in the middle of the stack [5, 15]. The helicity angle χ , which describes the character of domain walls as well as skyrmions, continuously rotates between the two extremes throughout the stack, with a characteristic profile $\chi(z)$, where z is the depth into the sample. In this case, the top CoFeB layer favors a Néel-type domain wall with a helicity angle of $\chi = 180^\circ$ or 0° , while the middle trilayer that hosts the Bloch point exhibits a Bloch-type domain wall with $\chi = \pm 90^\circ$. The bottom trilayer is again of Néel-type, but with χ changed by 180° from the surface [5, 23]. Introducing interfacial DMI moves the Bloch configuration in z [5, 15]. In nonzero external magnetic fields, a similar 3D magnetization characteristic is also expected for skyrmions.

Despite the predictions from micromagnetic simulations of Ta/CoFeB/MgO multilayer stacks being consistent with the CD-REXS measurements, a direct study of the depth-resolved magnetic environ-

ment in the stack has hitherto been lacking. Here we provide these measurements through an investigation of depth-dependent magnetism in the multilayer $[\text{Ta}(2)/\text{CoFeB}(1.5)/\text{MgO}(2)]_{16}/\text{Ta}(5)$ (thicknesses in nm) using low-energy muon-spin rotation (LE- μ^+ SR) [24–26]. Previous work [27–30] has shown that bulk μ^+ SR [24, 31] is a useful tool in the study of skyrmion systems and their dynamics, while LE- μ^+ SR has probed depth-dependent magnetism at interfaces [32] and the behavior of superconducting [33] and magnetic [34] superlattices. However, these studies do not address the evolution of the properties with depth within a repeating structure. Combining our measurements on $[\text{Ta}(2)/\text{CoFeB}(1.5)/\text{MgO}(2)]_{16}$ with energy-resolved CD-REXS, and interpreting them with support from micromagnetic simulations, we show here how the domain-wall angle and magnetic structure varies with depth, and reveal a crossover in magnetic properties as a function of depth.

II. EXPERIMENTAL AND COMPUTATIONAL DETAILS

The $[\text{Ta}(2)/\text{CoFeB}(1.5)/\text{MgO}(2)]_{16}/\text{Ta}(5)$ (thicknesses in nm) multilayered thin films were grown by magnetron sputtering onto Si wafers [5, 35]. A Ta layer was always chosen as the final layer to prevent oxidation. The base pressure of the deposition system was $<3 \times 10^{-6}$ Pa. The sputter gas, Ar, was used at a pressure of 0.3 Pa. The deposition rates for Ta, CoFeB, and MgO were 0.48, 0.30, and 0.05 Å/s respectively. A sputtering power of 100 W was used.

The CD-REXS experiments were carried out in the RASOR diffractometer on beamline I10 at the Diamond Light Source (UK). The CD-REXS patterns shown are obtained from the difference between the scattering intensities for left- and right-circularly polarized x-rays for varying photon energies around the Fe L_3 absorption edge. The dichroism extinction condition directly reveals the twisting angle of the magnetic structure averaged over the probed depth.

Micromagnetic simulations were performed using the Ubermag package [36], with OOMMF [37] as the computational backend. The same material parameters were used as in Ref. [5], with the layer thicknesses changed to be appropriate for our sample. The parameters included are exchange $A = 10$ pJm $^{-1}$, interfacial (C_{nv}) DMI $D = 0.4$ mJm $^{-2}$, and out-of-plane uniaxial anisotropy $K_u = 0.9$ MJm $^{-3}$, and the calculations also included demagnetisation in the Hamiltonian. In magnetic layers, the magnetic saturation was $M_s = 1.18$ MA m $^{-1}$. Open boundary conditions were employed on samples of lateral size 300×300 nm, and the system used a discretization of $4 \times 4 \times 0.5$ nm. The complete code used can be found in the Supplemental Material [17].

Low-energy (LE)- μ^+ SR measurements were carried out at the Swiss Muon Source, Paul Scherrer Institut,

Switzerland, using the LEM instrument, which allows the implantation depth of the muons to be altered by changing the energy of the incoming muons [25, 26]. Measurements were performed at 290 K, either in the ZF or TF geometry. Data analysis was carried out using both the WiMDA program [38], making use of the MINUIT algorithm [39] via the iminuit [40] Python interface for global refinement of parameters, and musrfit [41]. Stopping profiles of the muons in the multilayer stack were modeled using the TRIM.SP software [42]. A model of the multilayer stack was made in the software by inserting layers matching the density of each of the materials at the correct thickness to match the experimental system. TRIM.SP then calculates histograms of the stopping profiles for a particular incident muon energy; we varied this parameter to investigate the changes in stopping profiles. For these calculations, at all incident energies, the energy variance was set to 0.45 keV, and muons were incident perpendicular to the surface with a variance of 15° .

III. RESULTS & DISCUSSION

A. Circular dichroic resonant elastic x-ray scattering

We studied the depth-dependent character of the magnetic domain walls in the multilayer system $[\text{Ta}(2)/\text{CoFeB}(1.5)/\text{MgO}(2)]_{16}/\text{Ta}(5)$ on a Si substrate using CD-REXS [20–22, 43], which is sensitive to the twisting angle of spin spirals and skyrmions, and was previously applied to retrieve χ of a magnetic twisted domain state [21]. Figure 1(a) shows energy-dependent dichroic scattering patterns, obtained on the multilayer sample at room temperature and in zero applied magnetic field. The ring-like magnetic scattering patterns were obtained by integrating several azimuthal angles using the ϕ -axis of the diffractometer. The dichroic patterns feature a dividing vector that separates the blue and red regions of negative and positive dichroic contrast, governed by the dichroism extinction rule [20], see Fig. S2 in Ref. [17]. The azimuthal direction of the dividing vector uniquely reveals the value of χ [21] (Fig. S2 in Ref. [17]). For multilayer systems with a non-uniform $\chi(z)$ profile, the measured χ_m is the average χ from all trilayers with different weightings. Experimentally, by varying the photon energy across the Fe L_3 edge, or the x-rays incidence angle θ , the weight changes due to the varied sampling depth of the soft x-rays, leading to a different measured average χ_m [22, 23, 44]. For the investigated $[\text{Ta}(2)/\text{CoFeB}(1.5)/\text{MgO}(2)]_{16}/\text{Ta}(5)$ heterostructure, the attenuation length of the x-rays, Λ , is 79 nm at the Fe L_3 edge (707.8 eV) at normal incidence, and 152 nm off-edge (700 eV). The sampling depth varies with the angle between the x-ray beam and surface normal, α , as $\Lambda \cos(\alpha)/2$ [45]. A systematic variation of these parameters therefore provides a strategy for investigating the depth-dependent structural property of a 3D hybrid

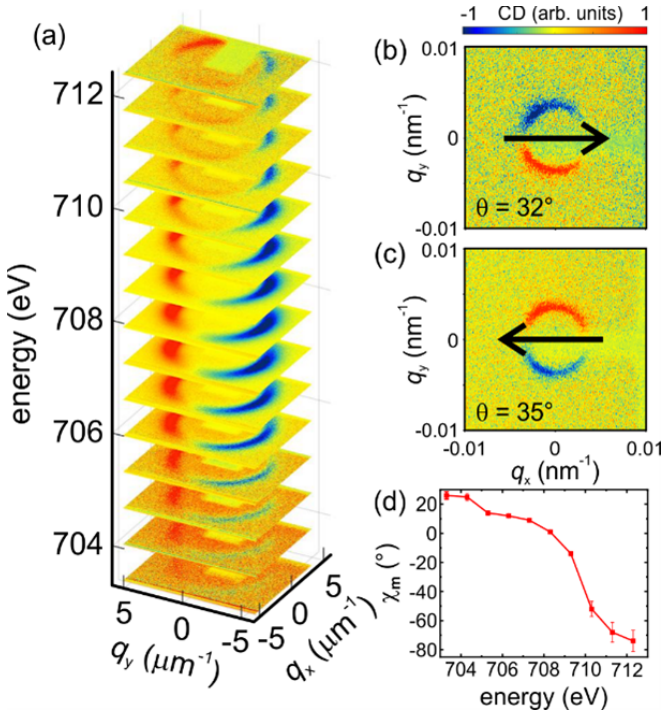


FIG. 1. CD-REXS patterns of the multilayered sample, measured at room temperature in zero magnetic field. (a) Energy-dependent CD-REXS patterns measured at $\theta = 12^\circ$. The individual patterns at the energies at which a helicity angle could be extracted are shown in Ref. [17]. (b,c) CD-REXS patterns measured at $\theta = 32^\circ$ and 35° , respectively, using a photon energy of 707.8 eV (at the Fe L_3 edge). (d) Energy dependence of the measured helicity angle χ_m across the L_3 absorption edge.

domain wall.

As can be seen in Fig. 1, the direction of the dividing vector undergoes a gradual change across the photon energy spectrum. Due to the complexity of the multilayered structure, the unambiguous determination of the $\chi(z)$ profile is not as straightforward as for chiral bulk magnets [22, 44], especially in combination with the variation of the incident angle. This is due to the appearance of complex interference effects in the multilayers, combined with the necessity to not only include layer-dependent absorption, but also dispersion. However, it is possible to obtain qualitative information about the $\chi(z)$ profile. In general, at photon energies far away from the Fe L_3 absorption edge, the soft x-ray attenuation length increases, while it is shorter near the resonance. Consequently, the top part of the multilayer which is closest to the surface contributes more to the total measured χ_m . In other words, if the $\chi(z)$ -profile monotonically changes between 180° and 0° as a function of depth, the dividing vector will slightly rotate when changing the photon energy across the Fe L_3 edge. This behavior is consistent with our observations in Fig. 1(a). Furthermore, the sampling depth can be changed over a larger range by varying the incident x-ray angle θ ($\theta = 90^\circ - \alpha$, where α is the scatter-

ing angle defined with respect to the surface normal) [17]. As shown in Figs. 1(b) and 1(c), by changing θ from 32° to 35° , the CD-REXS pattern reverses sign, suggesting the existence of a smoothly-varying 3D hybrid domain wall structure. Our CD-REXS results are therefore consistent with previous work on Ta/[CoFeB/MgO/Ta]₁₆ [5], and suggest Néel magnetic character near the surface and substrate, with Bloch-like character in the central region. A plot of χ_m as a function of energy, extracted from the CD-REXS image stack in Fig. 1(a), is shown in Fig. 1(d). Note that χ_m for larger energies is not defined, i.e., there is no clear dividing line in CD-REXS contrast as a result of the complex interference effects in the heterostructure. It is therefore beneficial to employ additional techniques, such as micromagnetics and LE- μ^+ SR, to further understand changes in the magnetic states with depth.

B. Micromagnetics

We have performed micromagnetic simulations of our multilayer system. Our sample has been converted to a micromagnetic model as shown in Fig. 2(a–b); in all layers apart from CoFeB we set the saturation magnetisation to zero, meaning that the magnetic layers interact only through the long-range dipolar field between them. We find that a magnetic state with chirality, in our case a skyrmion-like object, is lower in energy than a ferromagnetic configuration, suggesting that complex twisting magnetic configurations are the magnetic ground state. By initialising the system with a skyrmion before allowing it to relax, we are able to straightforwardly evaluate χ as a function of depth; the results are shown in Fig. 2(c). We find agreement with Ref. [5], specifically a Néel-type magnetic configuration on the top and bottom surfaces, with Bloch-like character in the middle of the stack. We were unable to simulate a skyrmion system with depth-independent helicity, suggesting that the depth-dependence significantly reduces the energy of the system. One might speculate that this depth-dependent helicity is inherent to a system that changes from semi-infinite (at the surfaces) to infinite (in the middle of the system) on the length scale of the interactions as it may minimise the free energy cost of the stray field.

C. Muon-spin rotation

With a consistent picture of the magnetism in Ta/[CoFeB/MgO/Ta]₁₆ arising from CD-REXS and micromagnetic simulations, we now turn to μ^+ SR, which is a powerful technique that allows one to learn about the magnetism from a local perspective. However, it is often challenging to interpret results from μ^+ SR, especially in complex magnetic systems. μ^+ SR depends intricately on the atomic configuration, with the location of the implanted muon with respect to the magnetic ions having significant impact on the field detected in a μ^+ SR exper-

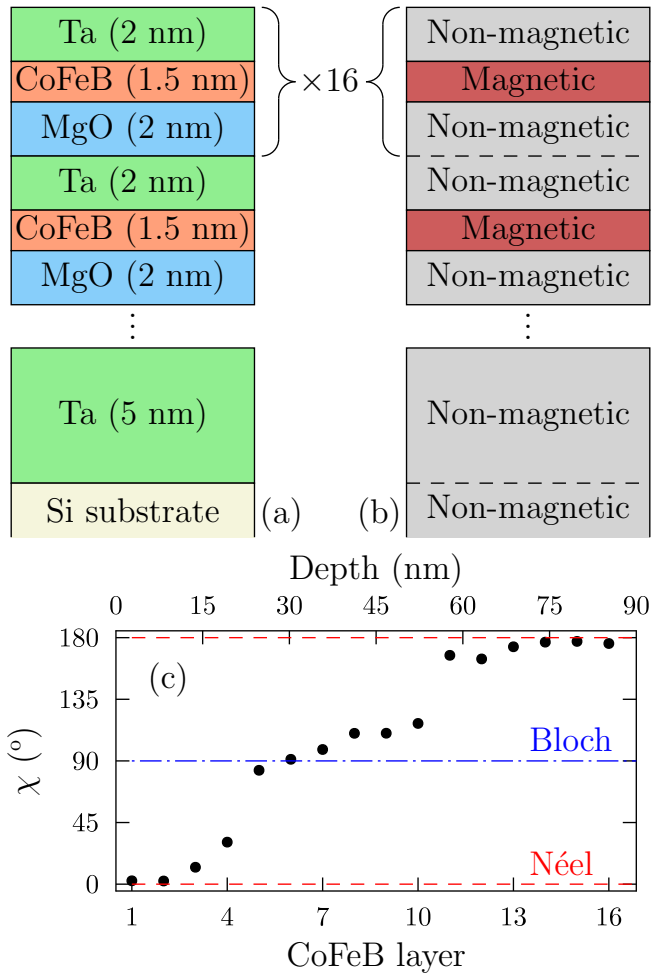


FIG. 2. (a) A diagram of the multilayer sample used in this work, with a demonstration of how this has been converted to a micromagnetic model in (b). The helicity of the multilayer system, χ , changes from Néel-type twisting at the top and bottom surfaces, to Bloch-like in the centre of the stack.

iment. Conversely, micromagnetics, by design, ignores atomic details of a material in favor of a continuum approximation. One would therefore not generally expect these two techniques to be complementary. In this case however, due to the existence of large volumes of non-magnetic material in which the muon will also stop and predominately feel the long-range dipolar field, the continuum limit in these regions is likely to provide a good estimate of the experimentally observed magnetic fields.

In a muon-spin rotation (μ^+ SR) experiment [24, 31] spin-polarized muons are implanted in a sample where they interact with the local magnetic field at the muon site. After, on average, $2.2 \mu\text{s}$, the muon decays into a positron and two neutrinos. By detecting these positrons, which are preferentially emitted in the direction of the muon-spin at the time of decay, we can track the polarization of the muon-spin ensemble.

Simulations of the muon stopping profile in our sample performed using TRIM.SP [42] [Fig. 3(a)] demonstrate

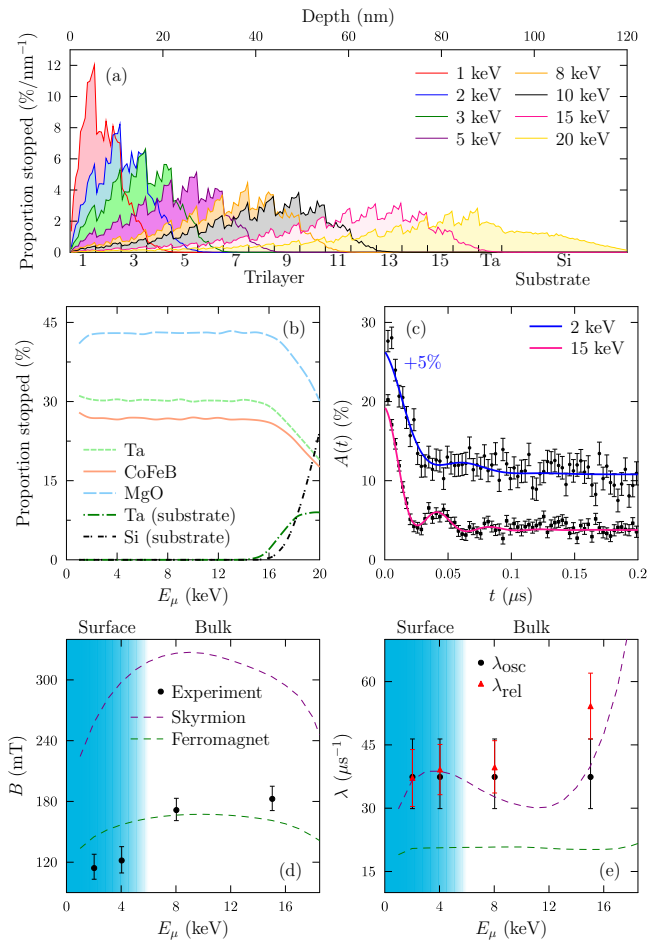


FIG. 3. (a–b) Muon stopping profiles: (a) implantation energy dependence, (b) the proportion of muons stopping in each layer type. (c) Typical ZF μ^+ SR spectra $A(t)$ with parameters extracted from fitting shown as points in (d–e). The dashed lines in (d–e) show the results from micromagnetic simulations of a ferromagnetic and a skyrmion-like state.

how the muons are distributed among the layers at different incident energies E_μ . Owing to the spread in the stopping profile, it is possible to distinguish the top layers from those deeper layers within the sample, although it is not possible to solely probe the layers of the sample nearest the substrate. The proportion of muons stopping in each layer type is shown in Fig. 3(b), and demonstrates that in the range $\simeq 2\text{--}16$ keV the proportion of muons in magnetic/non-magnetic layers does not change. In magnetic thin films, the dipolar field extends into non-magnetic layers with a length scale determined by the size of magnetic modulations [32, 46]; in our case, this is likely to be 10s of nm, matching the length scale of the skyrmions. There are sufficient muons stopping in all layers to probe the magnetism throughout the sample.

In zero applied field (ZF) we expect the system to host relatively disordered helical magnetic order. ZF μ^+ SR measurements at $T = 295$ K as a function of E_μ show the existence of two distinct regimes of behavior, classified by

different implantation depths. (For all measurements the muon spin is initially rotated approximately 10° out of the plane of the film.) The differences with E_μ can be seen in the muon asymmetry $A(t)$, [Fig. 3(c)]. To track the changes we parameterize the data [17, 38, 39, 41] using

$$A(t) = a_{\text{osc}}^{\text{ZF}} \exp(-\lambda_{\text{osc}} t) \cos(\gamma_\mu B t + \phi) + a_{\text{rel}}^{\text{ZF}} \exp(-\lambda_{\text{rel}} t) + \sum_{i=3}^4 a_{\text{bg},i} \exp(-\sigma_{\text{bg},i}^2 t^2). \quad (1)$$

Many of these parameters are energy-independent [17], leaving the term with amplitude $a_{\text{osc}}^{\text{ZF}}$ containing the majority of the information about the variation of the magnetic properties with depth, and the terms with amplitudes $a_{\text{bg},i}$ predominantly capturing background effects. The $a_{\text{osc}}^{\text{ZF}}$ term arises from muons that stop in sites where the muon spin and local field B are not parallel, leading to coherent spin precession. The relaxation rates depend both on the static distribution of fields at the muon site, and the dynamic fluctuations on the muon (MHz) timescale. The change in B with E_μ , which can be unambiguously extracted from the data irrespective of parameterization, is shown in Fig. 3(d); the internal field significantly increases from around 120 mT at 4 keV and below to around 180 mT at 8 keV and above. Conversely, the relaxation rates [Fig. 3(e)] remain approximately constant as a function of implantation energy.

There are two regimes evident in Fig. 3(d), with the measurements at 4 keV and below showing different behavior to those at 8 keV and above. Comparing with Fig. 3(a), we suggest a surface regime is formed from approximately the first 4 stacks nearest the surface, corresponding to a penetration depth up to $\simeq 22$ nm. At higher E_μ , the local field at the muon sites increases sharply in magnitude, suggesting a change in the magnetism.

To understand these changes, we compute the μ^+ SR spectra from our micromagnetic calculations (assuming no dynamic effects) for both a ferromagnetic and skyrmion-like configuration (that is, a skyrmion whose shape is affected by the finite size of the simulation) by weighting the calculated field at each depth by the relevant stopping probability for each E_μ . We are then able to extract the simulated internal field and relaxation rate by fitting the simulated spectra in the same way we fit the measured μ^+ SR spectra. The magnetic configurations explored in our simulations are picked as the simplest ones that allow us to describe the magnetic states found experimentally, since they represent the limiting cases, and allow us to explore the effect of introducing chirality. Specifically, the reported disordered helical groundstate of the material appears ferromagnetic on a short-length scale. On a longer length scale it appears to host disordered and chiral regions more akin to the simulated skyrmion-like configuration. The behaviour realized in the material is therefore anticipated to be something be-

tween the two simulations. We note that, due to the limited system size possible in our micromagnetic simulations, it is not feasible to directly explore the disordered helical groundstate on the length scales on which it is found to exist in experiment. However, we find that the results of small simulations of a helical state are consistent with those of our skyrmion-like configuration.

From our micromagnetic simulations we find that the calculated local field in the magnetic CoFeB layers is much higher and more varied than that in the non-magnetic layers. This will lead to fast precession with a large relaxation rate. However, the inherent experimental time-resolution of our measurement means that it is unlikely that we could observe these effects. Whilst the value of the field in the CoFeB layers in experiment is not expected to agree with the micromagnetic calculations (owing to this field being sensitively determined in the material by the local environment of the muon, which is not captured in a micromagnetic approach), we expect that a large, varied field will be experienced by the muon ensemble in these layers, hence preventing them from significantly contributing to the measured spectra. We therefore suggest that the measured spectra predominantly probe the stray dipolar field in the non-magnetic layers that arises from the ordered magnetism in the magnetic CoFeB layers.

The magnetic field extracted from the ferromagnetic micromagnetic calculation is consistent with the magnitude of that extracted from the experimental ZF- μ^+ SR spectra. The simulation shows a small increase in field as E_μ increases (likely to occur because the muon goes from seeing a ‘‘half-infinite’’ sample to an ‘‘infinite’’ one), although this increase is not as large as that observed experimentally. Conversely, although the field is much higher in the skyrmion-like calculation, it does show an increase much closer to that observed experimentally. The experimental relaxation rates, which are sensitive to the static distribution of magnetic fields seen by the muon, show little dependence on E_μ . Both simulated magnetic states predict relaxation rates with relatively little E_μ -dependence. However it is the relaxation from the skyrmion-like calculation whose order of magnitude is consistent with experiment in this case. (We also note that the disorder in the ferromagnetic calculation, and hence λ , is likely to be larger than in a well-ordered ferromagnetic sample due to the edge effects contributing significantly at this simulation size.) Taken together, these results imply that the material hosts a magnetic state that has some character of both calculations, not unlike the somewhat disordered helical state we expect. The large measured relaxation rate suggests a wide distribution of local magnetic fields at the muon site, consistent with a complex, twisting magnetic structure. Further, the significant increase in B with E_μ can only be explained by the micromagnetic simulation of the skyrmion-like configuration, where χ is depth-dependent. Moreover, our simulations demonstrate that the precise value of the μ^+ SR-fitting parameters will depend sensi-

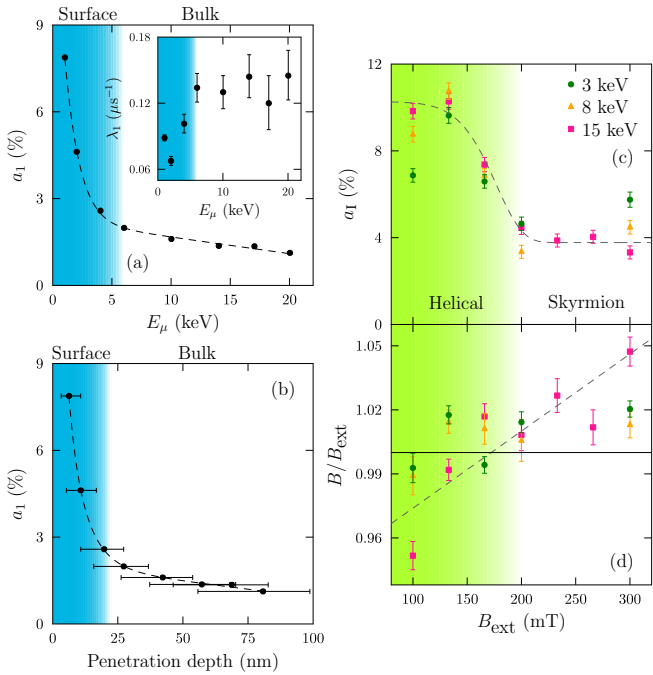


FIG. 4. (a) Energy dependence of parameters from fitting TF μ^+ SR at 10 mT, with a conversion to average muon penetration depth in (b). Error bars in (b) represent the asymmetric range in which 2/3rds of the muons stop according to the calculations in Fig. 3(a). (c–d) Field-dependent parameters from fitting TF μ^+ SR data, showing (c) the amplitude a_1 , and (d) the ratio of B to the applied field B_{ext} . Dashed lines are guides to the eye.

tively on the proportion of the sample that is domain wall- or ferromagnetic-like. Our μ^+ SR results are therefore consistent with micromagnetic simulations and CD-REXS, and suggest a quantitative agreement between the expected depth of changes in the magnetism.

To explore these changes further, TF μ^+ SR measurements were performed at 295 K as a function of E_μ in an applied magnetic field of 10 mT, applied perpendicular to the film, for which we expect the magnetic state to be relatively undisturbed. Representative TF μ^+ SR data can be found in the Supplemental Material [17]. For these data we fit the number of counts in each detector simultaneously, using the polarization function

$$P_x(t) = \sum_{i=1}^2 a_i \exp(-\lambda_i t) \cos(\gamma_\mu B t + \phi), \quad (2)$$

where, due to the difficulty in resolving two different fields at the muon site (in particular due to the large λ_2), and as we expect the shift in measured field to be small in magnetic thin films [47], we constrain the fits to share B between the two terms. We find many parameters to be energy-independent [17]. The energy-dependent parameters, a_1 and λ_1 , are shown in Fig. 4(a).

We interpret the two different terms as arising from muons stopping at different classes of muon site in the

sample. Since there is little change in the proportion of muons stopping in each different material as a function of E_μ [Fig. 3(b)], the results suggest the magnetic structure must change as a function of depth. The site contributing to the term with amplitude a_1 experiences a small internal field and has a small relaxation rate, leading to coherent precession in the applied magnetic field. This suggests these sites are sensitive mainly to regions of disordered magnetic field (where the average magnetic field cancels), such as domain wall-like regions. This weak relaxation rate λ_1 [inset of Fig. 4 (a)] increases with depth. Whilst it is tempting to interpret this in terms of the changes in the static magnetism that are supported by the results of our micromagnetic simulations (discussed above), it might be more reasonable to attribute such a weak relaxation rate [which is two orders of magnitude smaller than measured and simulated in Fig. 3(e)] to dynamics in the system. In this case, the increase in λ_1 would, in a fast-fluctuation limit, suggest that the frequency of dynamic fluctuations decreases at these sites with depth. Such behaviour could be expected since surface-dominated states have dynamics arising from rapid fluctuations on a relatively-short lengthscale (as the system tries to find a configuration that satisfies the constraint of the surface) to one where longer wavelength collective excitations dominate in the bulk of the material. As E_μ increases, the amplitude a_1 decreases, consistent with fewer surface-state muon-sites being realized with depth. We again see a crossover around trilayer 4 of the material. Although this appears relatively smooth in Fig. 3(a), this at least partially reflects the fact that the stopping profile is spread across several trilayers at each implantation energy. To elucidate this further, we have converted the implantation energy to a penetration depth using the results shown in Fig. 3(a); and present a_1 again as a function of this parameter [Fig. 4(b)]. We observe that a_1 remains approximately constant once the majority of muons are penetrating beyond around trilayer 4. The changes observed in the TF measurements coincide with the change in magnetic structure seen from the ZF results, implying that the same crossover with depth is responsible for both measurements. We therefore have a picture of (i) a static magnetic structure changing with depth (from those muon sites in large local magnetic field giving rise to the ZF signal), and (ii) the number of domain wall sites decreasing with depth, with the possibility that the dynamic fluctuation rate on the muon-timescale in these sites also decreases (from muon sites in regions with small local field giving rise to the wTF signal). For both types of muon site, the environment changes rapidly around trilayer 4.

To access the region of the phase diagram where skyrmions are stabilized as the majority phase, further TF μ^+ SR measurements were performed as a function of larger magnetic fields, at $T = 295$ K using implantation energies: 3, 8, and 15 keV. Note that the thickness of both the magnetic and non-magnetic layers strongly

affects the field at which skyrmions are stabilised (see Ref. [48]), which is a result we are also able to reproduce with our micromagnetic simulations. As such, the exact crossover field should be expected to be sample dependent. For these data $P_x(t) = a_I \exp(-\lambda_I t) \cos(\gamma_\mu B t + \phi_B) + a_{II} \exp(-\sigma_{II}^2 t^2)$ is found to describe the behavior over the entire dataset. Most parameters are found to be independent of applied magnetic field or arising from background effects [17], hence we focus on the term with amplitude a_I , arising from muons stopping in sites where the spin precess in a local field B , which is found to be close to the applied field. This implies we are again sensitive to the domain-wall sites where the average local field is small in these measurements. The field-dependent changes in a_I and B are shown in Fig. 4(c-d).

The proportion of muons stopping in the sample and giving coherent spin precession decreases as B_{ext} is increased [Fig. 4(c)]. This effect is approximately twice the size of that observed as a function of implantation energy in the low-TF measurements, suggesting that applied magnetic field leads to a more rapid decrease in the occurrence of these domain-wall environments compared to their variation with depth. This picture is supported by the results of x-ray ptychography measurements [5] that suggest just such a change in magnetic structure with out-of-plane magnetic field, such that skyrmions become the dominant magnetic defect above ~ 150 mT. The skyrmions represent a limiting case of the domain-wall structure, minimising the sample volume occupied by the low-field muon stopping sites. This is consistent with our measurement in which, around 180 mT, the amplitude parameter ceases changing, suggesting a crossover to a different regime. We therefore suggest that this crossover can be seen at all implantation energies, and that the plateau of a_I indicates the stabilization of skyrmions at each depth within the stack that we have probed.

There appears to be a weak dependence of the ratio B/B_{ext} with B_{ext} , Fig. 4(d). As B_{ext} increases, the enhancement of B becomes larger, from predominantly below the applied field, to above, most pronounced at 15 keV. The crossover between these regions appears to approximately coincide with the transition to skyrmion-dominated magnetic structures. The micromagnetic simulations suggest that the skyrmion-like states will exhibit a higher field at the muon site than when the system is ferromagnetic; it is therefore expect that crossover from a disordered helical state (which appears almost ferromagnetic on a short-length scale) to a disordered skyrmion state might also show a similar, albeit weaker, effect. Further, the reduction in a_I in the skyrmion-stabilized phase possibly reflects the behaviour of muons in sites

where the spin is relaxed too rapidly to be detected, reducing a_I . This is consistent with the response seen in bulk skyrmion systems [28–30], where the relaxation rate is enhanced at the center of the skyrmion lattice phase, even when the skyrmion lattice is not the majority phase.

IV. CONCLUSION

In summary, our LE- μ^+ SR and CD-REXS measurements identify changes in the magnetism of the [Ta(2)/CoFeB(1.5)/MgO(2)]₁₆/Ta(5) multilayer stack on a Si substrate as a function of both depth and applied field. Our micromagnetic simulations well explain these observations, and we have demonstrated the utility of cheap micromagnetic simulations for explaining μ^+ SR results when there is a large volume fraction of the sample that is non-magnetic. CD-REXS demonstrates the continuous evolution of the helicity angle with depth, while μ^+ SR shows that the magnetism in the top trilayers of the multilayer stack have a different static magnetic structure to those further from the surface. The trilayer at which this crossover is observed provides quantitative agreement with predictions from simulations [5, 23]. We also identify a decrease in the volume occupied by domain walls with both depth and applied magnetic field, with the latter undergoing a crossover to a regime dominated by skyrmions around 180 mT. Our work highlights the utility of the LE- μ^+ SR technique in studying multilayer skyrmion systems, providing unique insights into the depth dependence of the magnetic textures and their properties. Our findings confirm results from computational predictions, and paves the way for future investigations to experimentally verify a number of other computational works on technological applications of skyrmion-hosting systems. Determining the depth-dependence of the magnetic properties of multilayered systems is of paramount importance for their incorporation in device applications.

ACKNOWLEDGMENTS

Part of this work was carried out at the Paul Scherrer Institut, Switzerland; we are grateful for the provision of beamtime. The authors acknowledge Diamond Light Source for beamtime on beamline I10 under proposal SI-18898. The project was funded by EPSRC (UK) (Grant No: EP/N032128/1). M.N. Wilson acknowledges the support of the Natural Sciences and Engineering Research Council of Canada (NSERC). Research data from this paper will be made available via Durham Collections at <https://doi.org/10.15128/r2qn59q403m>.

[1] T. Lancaster, Skyrmions in magnetic materials, *Contemp. Phys.* **60**, 246 (2019).

[2] N. Nagaosa and Y. Tokura, Topological properties and dynamics of magnetic skyrmions, *Nature Nanotechnol.* **8**, 899 (2013).

- [3] W. Jiang, G. Chen, K. Liu, J. Zang, S. G. E. Te Velthuis, and A. Hoffmann, Skyrmions in magnetic multilayers, *Phys. Rep.* **704**, 1 (2017).
- [4] S. Zhang, J. Zhang, Y. Wen, E. M. Chudnovsky, and X. Zhang, Creation of a thermally assisted skyrmion lattice in Pt/Co/Ta multilayer films, *Appl. Phys. Lett.* **113**, 192403 (2018).
- [5] W. Li, I. Bykova, S. Zhang, G. Yu, R. Tomasello, M. Carpentieri, Y. Liu, Y. Guang, J. Gräfe, M. Weigand, D. M. Burn, G. van der Laan, T. Hesjedal, Z. Yan, J. Feng, C. Wan, J. Wei, X. Wang, X. Zhang, H. Xu, C. Guo, H. Wei, G. Finocchio, X. Han, and G. Schütz, Anatomy of skyrmionic textures in magnetic multilayers, *Adv. Mater.* **31**, 1807683 (2019).
- [6] E. Burgos-Parra, Y. Sassi, W. Legrand, F. Ajejas, C. Léveillé, P. Gargiani, M. Valvidares, N. Reyren, V. Cros, N. Jaouen, *et al.*, Probing of three-dimensional spin textures in multilayers by field dependent x-ray resonant magnetic scattering, *Scientific Reports* **13**, 11711 (2023).
- [7] S. Flewett, E. Burgos-Parra, M. G. Strelow, Y. Sassi, C. Léveillé, F. Ajejas, N. Reyren, and N. Jaouen, General treatment of off-specular resonant soft x-ray magnetic scattering using the distorted-wave born approximation: Numerical algorithm and experimental studies with hybrid chiral domain structures, *Physical Review B* **103**, 184401 (2021).
- [8] P. Milde, D. Köhler, J. Seidel, L. Eng, A. Bauer, A. Chacon, J. Kindervater, S. Mühlbauer, C. Pfleiderer, S. Buhrandt, *et al.*, Unwinding of a skyrmion lattice by magnetic monopoles, *Science* **340**, 1076 (2013).
- [9] M. E. Henderson, B. Heacock, M. Bleuel, *et al.*, Three-dimensional neutron far-field tomography of a bulk skyrmion lattice, *Nat. Phys.* 10.1038/s41567-023-02175-4 (2023).
- [10] D. Wolf, S. Schneider, U. K. Röbller, A. Kovács, M. Schmidt, R. E. Dunin-Borkowski, B. Büchner, B. Rellinghaus, and A. Lubk, Unveiling the three-dimensional magnetic texture of skyrmion tubes, *Nature nanotechnology* **17**, 250 (2022).
- [11] S. Seki, M. Suzuki, M. Ishibashi, R. Takagi, N. Khanh, Y. Shiota, K. Shibata, W. Koshibae, Y. Tokura, and T. Ono, Direct visualization of the three-dimensional shape of skyrmion strings in a noncentrosymmetric magnet, *Nature materials* **21**, 181 (2022).
- [12] C. Donnelly, K. L. Metlov, V. Scagnoli, M. Guizar-Sicairos, M. Holler, N. S. Bingham, J. Raabe, L. J. Heyderman, N. R. Cooper, and S. Gliga, Experimental observation of vortex rings in a bulk magnet, *Nature Physics* **17**, 316 (2021).
- [13] K. Witte, A. Späth, S. Finizio, C. Donnelly, B. Watts, B. Sarafimov, M. Odstrcil, M. Guizar-Sicairos, M. Holler, R. H. Fink, *et al.*, From 2D STXM to 3D imaging: Soft X-ray laminography of thin specimens, *Nano letters* **20**, 1305 (2020).
- [14] C. Donnelly, M. Guizar-Sicairos, V. Scagnoli, S. Gliga, M. Holler, J. Raabe, and L. J. Heyderman, Three-dimensional magnetization structures revealed with x-ray vector nanotomography, *Nature* **547**, 328 (2017).
- [15] W. Legrand, J.-Y. Chauleau, D. Maccariello, N. Reyren, S. Collin, K. Bouzehouane, N. Jaouen, V. Cros, and A. Fert, Hybrid chiral domain walls and skyrmions in magnetic multilayers, *Sci. Adv.* **4**, eaat0415 (2018).
- [16] M. Grelier, F. Godel, A. Vecchiola, S. Collin, K. Bouzehouane, A. Fert, V. Cros, and N. Reyren, Three-dimensional skyrmionic cocoons in magnetic multilayers, *Nature communications* **13**, 6843 (2022).
- [17] See supplemental material for information on the different experimental techniques, more representative data, and more detailed information of the fitting of experimental data that would allow one to recreate our analysis. the complete micromagnetic code can also be found.
- [18] G. van der Laan, Soft x-ray resonant magnetic scattering of magnetic nanostructures, *C. R. Physique* **9**, 570 (2008).
- [19] S. L. Zhang, G. van der Laan, and T. Hesjedal, Direct experimental determination of the topological winding number of skyrmions in Cu_2OSeO_3 , *Nat. Commun.* **8**, 14619 (2017).
- [20] S. L. Zhang, G. van der Laan, and T. Hesjedal, Direct experimental determination of spiral spin structures via the dichroism extinction effect in resonant elastic soft x-ray scattering, *Phys. Rev. B* **96**, 094401 (2017).
- [21] S. Zhang, G. van der Laan, W. Wang, A. Haghighirad, and T. Hesjedal, Direct observation of twisted surface skyrmions in bulk crystals, *Phys. Rev. Lett.* **120**, 227202 (2018).
- [22] S. Zhang, G. van der Laan, J. Müller, L. Heinen, M. Garst, A. Bauer, H. Berger, C. Pfleiderer, and T. Hesjedal, Reciprocal space tomography of 3D skyrmion lattice order in a chiral magnet, *Proc. Natl. Acad. Sci. U.S.A.* **115**, 6386 (2018).
- [23] Y. Guang, K. Ran, J. Zhang, Y. Liu, S. Zhang, X. Qiu, Y. Peng, X. Zhang, M. Weigand, J. Gräfe, G. Schütz, G. van der Laan, T. Hesjedal, S. Zhang, G. Yu, and X. Han, Superposition of emergent monopole and antimonopole in CoTb thin films, *Phys. Rev. Lett.* **127**, 217201 (2021).
- [24] S. J. Blundell, R. De Renzi, T. Lancaster, and F. L. Pratt, *Muon Spectroscopy: An Introduction* (Oxford University Press, Oxford, 2022).
- [25] T. Prokscha, E. Morenzoni, K. Deiters, F. Foroughi, D. George, R. Kobler, A. Suter, and V. Vrankovic, The new $\mu\text{e}4$ beam at PSI: A hybrid-type large acceptance channel for the generation of a high intensity surface-muon beam, *Nucl. Instrum. Meth. A* **595**, 317 (2008).
- [26] E. Morenzoni, H. Glückler, T. Prokscha, H. P. Weber, E. M. Forgan, T. J. Jackson, H. Luetkens, C. Niedermayer, M. Pleines, M. Birke, A. Hofer, J. Litterst, T. Riseman, and G. Schatz, Low-energy μSR at PSI: present and future, *Physica B: Cond. Matter* **289**, 653 (2000).
- [27] T. Lancaster, R. C. Williams, I. O. Thomas, F. Xiao, F. L. Pratt, S. J. Blundell, J. C. Loudon, T. Hesjedal, S. J. Clark, P. D. Hatton, M. Ciomaga Hatnean, D. S. Keeble, and G. Balakrishnan, Transverse field muon-spin rotation signature of the skyrmion-lattice phase in Cu_2OSeO_3 , *Phys. Rev. B* **91**, 224408 (2015).
- [28] K. J. A. Franke, B. M. Huddart, T. J. Hicken, F. Xiao, S. J. Blundell, F. L. Pratt, M. Crisanti, J. A. T. Barker, S. J. Clark, A. Štefančič, M. Ciomaga Hatnean, G. Balakrishnan, and T. Lancaster, Magnetic phases of skyrmion-hosting $\text{GaV}_4\text{S}_{8-y}\text{Se}_y$ ($y = 0, 2, 4, 8$) probed with muon spectroscopy, *Phys. Rev. B* **98**, 054428 (2018).
- [29] T. J. Hicken, S. J. R. Holt, K. J. A. Franke, Z. Hawkhead, A. Štefančič, M. N. Wilson, M. Gomilšek, B. M. Huddart, S. J. Clark, M. R. Lees, F. L. Pratt, S. J. Blundell,

- G. Balakrishnan, and T. Lancaster, Magnetism and néel skyrmion dynamics in $\text{GaV}_4\text{S}_{8-y}\text{Se}_y$, *Phys. Rev. Res.* **2**, 032001(R) (2020).
- [30] T. J. Hicken, M. N. Wilson, K. J. A. Franke, B. M. Huddart, Z. Hawkhead, M. Gomilšek, S. J. Clark, F. L. Pratt, A. Štefančič, A. E. Hall, M. Ciomega Hatnean, G. Balakrishnan, and T. Lancaster, Megahertz dynamics in skyrmion systems probed with muon-spin relaxation, *Phys. Rev. B* **103**, 024428 (2021).
- [31] S. J. Blundell, Spin-polarized muons in condensed matter physics, *Contemp. Phys.* **40**, 175 (1999).
- [32] J. A. Krieger, Y. Ou, M. Caputo, A. Chikina, M. Döbeli, M.-A. Husanu, I. Keren, T. Prokscha, A. Suter, C.-Z. Chang, *et al.*, Do topology and ferromagnetism cooperate at the $\text{EuS}/\text{Bi}_2\text{Se}_3$ interface?, *Physical Review B* **99**, 064423 (2019).
- [33] A. Suter, E. Morenzoni, T. Prokscha, B. M. Wojek, H. Luetkens, G. Nieuwenhuys, A. Gozar, G. Logvenov, and I. Božović, Two-dimensional magnetic and superconducting phases in metal-insulator $\text{La}_2 - x\text{Sr}_x\text{CuO}_4$ superlattices measured by muon-spin rotation, *Phys. Rev. Lett.* **106**, 237003 (2011).
- [34] A. V. Boris, Y. Matiks, E. Benckiser, A. Frano, P. Popovich, V. Hinkov, P. Wochner, M. Castro-Colin, E. Detemple, V. K. Malik, C. Bernhard, T. Prokscha, A. Suter, Z. Salman, E. Morenzoni, G. Cristiani, H.-U. Habermeier, and B. Keimer, Dimensionality control of electronic phase transitions in nickel-oxide superlattices, *Science* **332**, 937 (2011).
- [35] D. M. Burn, S. L. Zhang, G. Q. Yu, Y. Guang, H. J. Chen, X. P. Qiu, G. van der Laan, and T. Hesjedal, Depth-resolved magnetization dynamics revealed by x-ray reflectometry ferromagnetic resonance, *Phys. Rev. Lett.* **125**, 137201 (2020).
- [36] H. Fangohr, M. Lang, S. J. R. Holt, S. A. Pathak, K. Zulfiqar, and M. Beg, Vision for unified micromagnetic modeling (UMM) with Ubermag, *AIP Advances* **14**, 015138 (2024), <https://pubs.aip.org/aip/adv/article-pdf/doi/10.1063/9.0000661/18702426/015138.1.9.0000661.pdf>.
- [37] M. J. Donahue and D. G. Porter, Oomf user's guide, version 1.0 (1999).
- [38] F. L. Pratt, WiMDA: a muon data analysis program for the Windows PC, *Physica B: Conden. Matter* **289**, 710 (2000).
- [39] F. James and M. Roos, MINUIT: a system for function minimization and analysis of the parameter errors and corrections, *Comp. Phys. Comm.* **10**, 343 (1975).
- [40] iminuit team, iminuit – a python interface to minuit, <https://github.com/scikit-hep/iminuit> (Accessed: 04-10-2022).
- [41] A. Suter and B. Wojek, Musrfit: a free platform-independent framework for μsr data analysis, *Phys. Procedia* **30**, 69 (2012).
- [42] E. Morenzoni, H. Glückler, T. Prokscha, R. Khasanov, H. Luetkens, M. Birke, E. Forgan, C. Niedermayer, and M. Pleines, Implantation studies of keV positive muons in thin metallic layers, *Nucl. Instrum. Meth. B* **192**, 254 (2002).
- [43] G. van der Laan and A. I. Figueroa, X-ray magnetic circular dichroism—a versatile tool to study magnetism, *Coord. Chem. Rev.* **277**, 95 (2014).
- [44] K. Ran, Y. Liu, H. Jin, Y. Shangguan, Y. Guang, J. Wen, G. Yu, G. van der Laan, T. Hesjedal, and S. Zhang, Axially bound magnetic skyrmions: Glueing topological strings across an interface, *Nano Lett.* **22**, 3737 (2022).
- [45] G. van der Laan, S. L. Zhang, and T. Hesjedal, Depth profiling of 3D skyrmion lattices in a chiral magnet – A story with a twist, *AIP Adv.* **11**, 015108 (2021).
- [46] E. Tsymbal, Evaluation of the magnetic dipolar fields from layered systems on atomic scale, *Journal of magnetism and magnetic materials* **130**, L6 (1994).
- [47] Z. Salman and S. Blundell, Proximal magnetometry of monolayers of magnetic moments, *Physics Procedia* **30**, 168 (2012).
- [48] P. Santos, P. Araujo, D. Sørensen, F. Matos, P. P. Freitas, and S. Cardoso, Micromagnetic simulations of cofeb/mgo perpendicular stacks for sensor applications, *IEEE Transactions on Magnetics* 10.1109/TMAG.2023.3285419 (2023).